Metal-optic cavity for a high efficiency sub-fF Germanium photodiode on a Silicon waveguide

Ryan Going,[1,*] Myung-Ki Kim,[1,2] and Ming C Wu[1]

[1]*Department of Electrical Engineering and Computer Science, University of California, Berkeley, Berkeley, CA 94720, USA*

[2]*Currently at Department of Electrical Engineering, California Institute of Technology, Pasadena, CA 91125, USA*

[*]*rwgoing@berkeley.edu*

Abstract: We propose two designs of nanoscale sub-fF germanium photodiodes which are efficiently integrated with silicon waveguides. The metal-optic cavities are simulated with the finite difference time domain method and optimized using critical coupling concepts. One design is for a metal semiconductor metal photodiode with <200 aF capacitance, 39% external quantum efficiency, and 0.588 $(\lambda/n)^3$ cavity volume at 1.5μm wavelength. The second design is for a vertical p-i-n photodiode with <100 aF capacitance, 51% external quantum efficiency, and 0.804 $(\lambda/n)^3$ cavity volume. Both designs make use of CMOS compatible materials germanium and aluminum metal for potential future monolithic integration with silicon photonics.

OCIS codes: (230.5160) Photodetectors; (260.3910) Metal optics; (130.3990) Micro-optical devices.

References and links

1. D. A. B. Miller, "Device requirements for optical interconnects to silicon chips," Proc. IEEE **97**(7), 1166–1185 (2009).
2. M. A. Taubenblatt, "Optical interconnects for high-performance computing," J. Lightwave Technol. **30**(4), 448–457 (2012).
3. M. Rouviere, M. Halbwax, J. Cercus, E. Cassan, L. Vivien, D. Pascal, M. Heitzmann, J.-M. Hartmann, and S. Laval, "Integration of germanium waveguide photodetectors for intrachip optical interconnects," Opt. Eng. **44**, 075402 (2005).
4. R. F. Potter, "Germanium (Ge)," in *Handbook of Optical Constants of Solids*, Palik, E. D., ed. (Academic Press, 1985), Vol. 1, pp. 465–478.
5. C. T. DeRose, D. C. Trotter, W. A. Zortman, A. L. Starbuck, M. Fisher, M. R. Watts, and P. S. Davids, "Ultra compact 45 GHz CMOS compatible Germanium waveguide photodiode with low dark current," Opt. Express **19**(25), 24897–24904 (2011).
6. L. Chen and M. Lipson, "Ultra-low capacitance and high speed germanium photodetectors on silicon," Opt. Express **17**(10), 7901–7906 (2009).
7. J. Wang and S. Lee, "Ge-photodetectors for Si-based optoelectronic integration," Sensors (Basel) **11**(12), 696–718 (2011).
8. O. Dosunmu, D. Cannon, M. Emsley, B. Ghyselen, J. Liu, L. Kimerling, and M. Unlu, "Resonant cavity enhanced Ge photodetectors for 1550 nm operation on reflecting Si substrates," IEEE J. Sel. Top. Quantum Electron. **10**(4), 694–701 (2004).
9. L. Tang, S. E. Kocabas, S. Latif, A. K. Okyay, D.-S. Ly-Gagnon, K. C. Saraswat, and D. A. B. Miller, "Nanometre-scale germanium photodetector enhanced by a near-infrared dipole antenna," Nat. Photonics **2**(4), 226–229 (2008).
10. F.-F. Ren, K.-W. Ang, J. Ye, M. Yu, G.-Q. Lo, and D.-L. Kwong, "Split Bull's eye shaped aluminum antenna for plasmon-enhanced nanometer scale germanium photodetector," Nano Lett. **11**(3), 1289–1293 (2011).
11. M.-K. Kim, A. M. Lakhani, and M. C. Wu, "Efficient waveguide-coupling of metal-clad nanolaser cavities," Opt. Express **19**(23), 23504–23512 (2011).
12. M. T. Hill, Y.-S. Oei, B. Smalbrugge, Y. Zhu, T. de Vries, P. J. van Veldhoven, F. W. M. van Otten, T. J. Eijkemans, J. P. Turkiewicz, H. de Waardt, E. J. Geluk, S.-H. Kwon, Y.-H. Lee, R. Notzel, and M. K. Smit, "Lasing in metallic-coated nanocavities," Nat. Photonics **1**(10), 589–594 (2007).
13. K. Ding, M. T. Hill, Z. C. Liu, L. J. Yin, P. J. van Veldhoven, and C. Z. Ning, "Record performance of electrical injection sub-wavelength metallic-cavity semiconductor lasers at room temperature," Opt. Express **21**(4), 4728–4733 (2013).

#194169 - $15.00 USD Received 22 Jul 2013; revised 3 Sep 2013; accepted 3 Sep 2013; published 16 Sep 2013

14. M. T. Hill, M. Marell, E. S. P. Leong, B. Smalbrugge, Y. Zhu, M. Sun, P. J. van Veldhoven, E. J. Geluk, F. Karouta, Y.-S. Oei, R. Nötzel, C.-Z. Ning, and M. K. Smit, "Lasing in metal-insulator-metal sub-wavelength plasmonic waveguides," Opt. Express **17**(13), 11107–11112 (2009).
15. Q. Ding, A. Mizrahi, Y. Fainman, and V. Lomakin, "Dielectric shielded nanoscale patch laser resonators," Opt. Lett. **36**(10), 1812–1814 (2011).
16. Y. Liu, M. Deal, and J. Plummer, "Rapid melt growth of Germanium crystals with self-aligned microcrucibles on Si substrates," J. Electrochem. Soc. **152**(8), G688–G693 (2005).
17. S. Assefa, F. Xia, S. W. Bedell, Y. Zhang, T. Topuria, P. M. Rice, and Y. A. Vlasov, "CMOS-integrated high-speed MSM germanium waveguide photodetector," Opt. Express **18**(5), 4986–4999 (2010).
18. S. Assefa, F. Xia, and Y. A. Vlasov, "Reinventing Germanium avalanche photodetector for nanophotonic on-chip optical interconnects," Nature **464**(7285), 80–84 (2010).
19. H.-Y. Yu, S. Ren, W. S. Jung, A. K. Okyay, D. A. B. Miller, and K. C. Saraswat, "High-efficiency p-i-n photodetectors on selective-area-grown Ge for monolithic integration," IEEE Electron Device Lett. **30**(11), 1161–1163 (2009).
20. D. Y. Smith, E. Shiles, and M. Inokuti, "The Optical Properties of Metallic Aluminum," in *Handbook of Optical Contstants of Solids*, Palik, E. D., ed. (Academic Press, 1985), Vol. 1, pp. 369–406.
21. D. K. Schroder, R. N. Thomas, and J. C. Swartz, "Free carrier absorption in Silicon," IEEE J. Solid-State Circuits **13**(1), 180–187 (1978).
22. H. A. Haus, *Waves and Fields in Optoelectronics* (Prentice Hall, 1983).
23. M. Soltani, S. Yegnanarayanan, Q. Li, and A. Adibi, "Systematic engineering of waveguide-resonator coupling for silicon microring/microdisk/racetrack resonators: theory and experiment," IEEE J. Quantum Electron. **46**(8), 1158–1169 (2010).
24. S. Jongthammanurak, J. Liu, K. Wada, D. D. Cannon, D. T. Danielson, D. Pan, L. C. Kimerling, and J. Michel, "Large electro-optic effect in tensile strained Ge-on-Si films," Appl. Phys. Lett. **89**(16), 161115 (2006).
25. G. Roelkens, L. Liu, D. Liang, R. Jones, A. Fang, B. Koch, and J. Bowers, "III-V/silicon photonics for on-chip and inter-chip optical interconnects," Laser Photon. Rev. **4**(6), 751–779 (2010).

1. Introduction

Silicon photonics is currently a popular contender for replacing electrical interconnects for both inter- and intra-chip communications [1,2]. One of the key requirements for this disruptive replacement to occur is for the optical link to reduce its energy consumption to less than 10 fJ/bit [1]. To achieve this figure, there is a need for reduction in total photons/bit used to communicate, necessitating a highly sensitive photoreceiver, requiring a reduction in photodiode capacitance. While shrinking the physical dimensions of the photodiode will reduce its capacitance, doing so can severely reduce the quantum efficiency of the device by shrinking its absorptive area. This is compounded by the fact that the most likely material candidate for the photodiode is germanium due to its CMOS compatibility [3], however its absorption coefficient is relatively weak at 1550 nm [4]. The smallest capacitance photodiode currently reported is 1.2 fF with a quantum efficiency of nearly 67% [5], while a slightly higher capacitance diode, 2.4 fF, has also been developed but with much higher, 95%, quantum efficiency [6]. These are also some of the fastest reported germanium photodiodes since reducing RC delay increases overall speed [7].

Several methods have been used previously for enhancing the absorption in photodiodes such as creating resonant cavities [8] and metal antennas [9,10]. However the resonant cavities previously described are still rather bulky, 130 fF capacitance [8], and rely on normal incident illumination, while modern silicon photonics utilizes silicon waveguides for light transport. The antenna coupled photodiodes, while having extremely low capacitance, 8 aF in one case, have extremely low quantum efficiency (<1%). This is partially due to issues related to pushing the limits of current fabrication, but also due to their fundamental reliance on plasmonic modes, which utilizes electrical energy being present in the metal of the antenna, which is extremely absorptive at optical frequencies. Metal-optic nanocavities can be an alternative, which have recently been proposed for efficient nanoscale lasers integrated onto silicon waveguides [11–15]. By relying on dielectric modes using the metal as a reflector, these cavities minimize metal losses, are extremely compact, and have been demonstrated to couple well to waveguide modes.

In this paper, we report on two aluminum-clad metal-optic nanocavities which strongly enhance light absorption in subwavelength germanium at 1500 nm for sub-fF photodiodes.

#194169 - $15.00 USD Received 22 Jul 2013; revised 3 Sep 2013; accepted 3 Sep 2013; published 16 Sep 2013

Detailed designs and simulations for both cavities are reported, along with a detailed analysis of their performance and design trade-offs using coupled mode theory. One design is for a metal semiconductor metal photodiode, with a capacitance of <200 aF and 39% external quantum efficiency. The second is a p-i-n photodiode with capacitance <100 aF and 51% external quantum efficiency.

2. Device design

2.1 Metal semiconductor metal (MSM) photodiode

The proposed device, shown in Fig. 1(a), shows the metal clad cavity sitting on top of a terminated silicon waveguide. The primary feature seen is that the entire cavity is coated in aluminum, excepting a thin strip removed from the sidewalls and top, forming two electrically isolated metal walls which function as the contacts for the device. It sits on a 400 nm × 220 nm silicon waveguide on oxide. The waveguide couples evanescently through the bottom of the cavity. Figure 1(b) shows a cut-away running through the middle of the device along the waveguide. A small (400 nm × 400 nm × 180 nm) block of germanium is the absorber for the photodiode. The dimensions of the germanium are what primarily determine the cavity mode and the resonant wavelength. The split metal walls contact the top of the germanium directly for photocurrent extraction. The germanium can be undoped for a metal-semiconductor-metal photodiode, or laterally doped for a p-i-n photodiode. Surrounding the germanium on the sides is a thin (100 nm) layer of oxide, which isolates the mode in the germanium from the metal, reducing the metal absorption losses. Finally, the silicon nitride spacer controls the coupling between the waveguide and the cavity mode. By changing the thickness of this layer, critical coupling can be achieved, optimizing the absorption. This spacer can also be oxide, however silicon nitride was chosen for fabrication considerations. In both cases, it is possible to obtain relaxed and defect-free single-crystal germanium on this layer by rapid melt growth [16], which has been demonstrated to be relatively easy and reliable [17,18]. To incorporate rapid melt growth, an island of silicon, electrically and optically isolated from the device, would be needed to act as the crystal seed. The removal of the excess germanium and seeding region would be a required part of the fabrication.

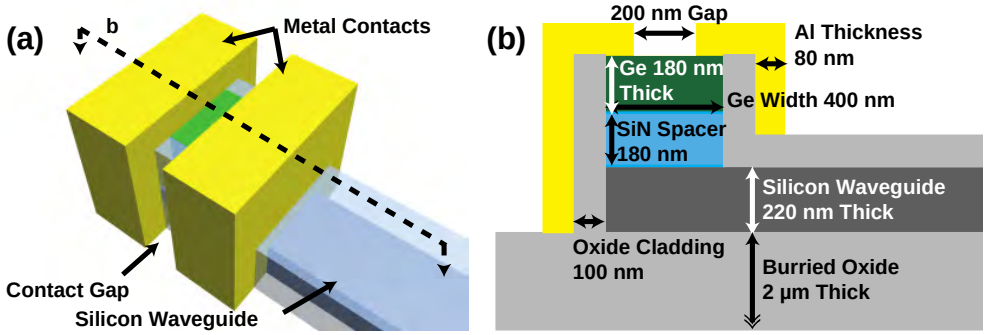

Fig. 1. (a) 3-D drawing of the proposed device showing the metal-clad box sitting on the terminated input waveguide. Splitting down the center of the waveguide shows (b) the interior components of the cavity and device can be seen.

2.2 Vertical p-i-n photodiode

The device drawn in Fig. 2 is very similar to that of the MSM structure with a few noticeable differences. Primarily, the device assumes vertical doping of the germanium, which requires contact through the bottom. By utilizing selective germanium growth on silicon, which has recently been developed to produce almost defect free germanium [5,19], the bottom contact can in fact be made by the silicon waveguide. In order to make contact without disturbing the

#194169 - $15.00 USD Received 22 Jul 2013; revised 3 Sep 2013; accepted 3 Sep 2013; published 16 Sep 2013

incoming waveguide mode, the waveguide is extended laterally from under the germanium region where aluminum is deposited on doped silicon, much like a truncated version of the waveguide integrated germanium photodiodes seen recently [5]. The metal box surrounding it is unbroken, and contacts the germanium indirectly through a poly-silicon layer, which serves to both isolate the mode from the metal and enhance the coupling to the cavity.

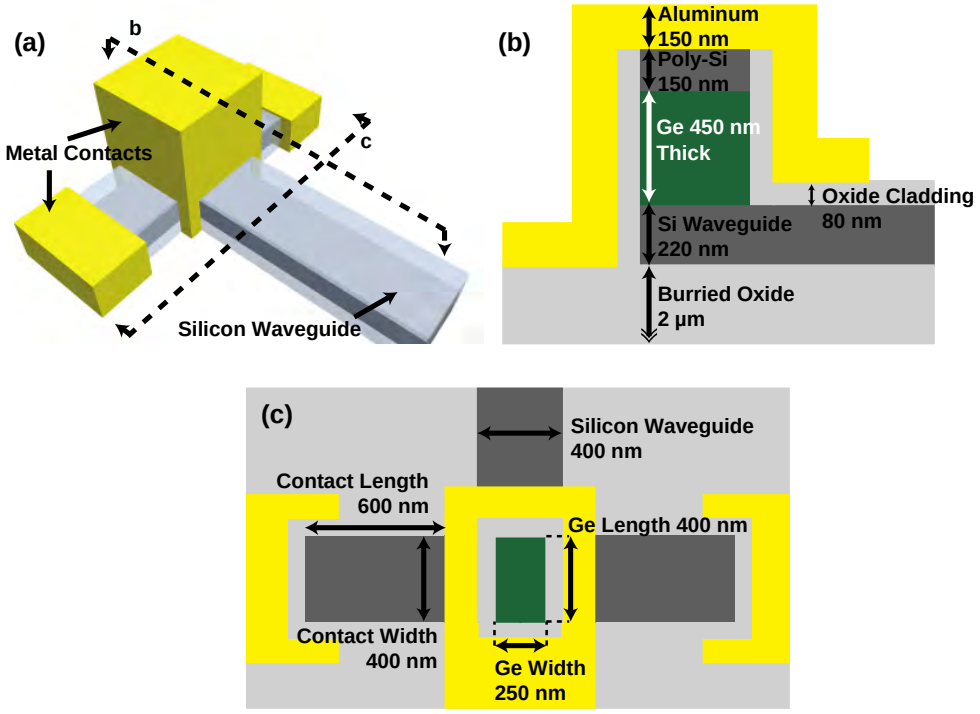

Fig. 2. (a) 3-D drawing of the vertical p-i-n photodiode showing aluminum metal totally enclosing the active germanium. (b) A cut down the center of the input waveguide shows the internal cavity with top and bottom silicon contacts, while (c) a slice in the substrate plane reveals the lateral cavity dimensions as well as the side silicon contacts.

The dimensions of germanium are comparable to the previous design as seen from Fig. 2. One key difference is the increased germanium thickness. Because there is no longer an oxide or nitride layer separating the germanium from the waveguide, it must be much thicker than before to prevent overcoupling to the cavity. The oxide surrounding the Ge is 80 nm, and the metal is 150 nm thick, however it should be noted that with this design the metal can be as thick as desired, the only requirement being thicker than the skin depth. Finally the silicon contacts on the side of the device are 400 nm wide and about 750 nm long. It will be shown later that the length of these contacts is critical to the device performance because they act as additional waveguides for the cavity to couple to and thus much be chosen with care. Finally since this device is designed to be a p-i-n structure, both the germanium and the silicon must be doped, and since high doping are required for good contact, the free carrier absorption of silicon will begin to play a role in the device performance.

3. Optimization of quantum efficiency

In order to optimize the structures for high quantum efficiencies, we simulated the devices using the finite difference time domain (FDTD) solver CST Microwave Studio. Both germanium and aluminum index of refraction and absorption coefficient values were taken from the Handbook of optical constants of solids [4,20]. These values assume single crystal germanium, and aluminum evaporated or sputtered under high vacuum. Both simulated

#194169 - $15.00 USD Received 22 Jul 2013; revised 3 Sep 2013; accepted 3 Sep 2013; published 16 Sep 2013

devices are air clad. To account for free carrier absorption associated with doping in the p-i-n device, both the polysilicon top contact, and bottom silicon waveguide are given an absorption coefficient of 300 cm^{-1}, which at 1500 nm, corresponds to a doping concentration of $5x10^{19}$ cm^{-3} [21].

In calculating the quantum efficiency of the device, we rely on two efficiency measures, η_{abs} and η_{coup}, which are the internal mode absorption efficiency and the external coupling efficiency, respectively. We define the quantum efficiency as the product of the two. We ingore in this analysis the internal electrical efficiency, which can reduce the total extracted photocurrent due to recombination from poor contacts, defect traps, and other imperfections in the electrical design. In the entirety of this paper, all mentions of quantum efficiency assume that all absorbed photons produce electrons and holes that contribute to photocurrent. Thus the reported quantum efficiency describes the ratio of photons absorbed in the germanium divided by the number of photons incident on device from the silicon waveguide.

The internal mode absorption efficiency is calculated using coupled mode theory (CMT) [22] to calculate the absorption for a given mode using the relevant Q-factors. In this case we use the radiation Q of the cavity, Q_{rad}, the Q from metal absorption, Q_{metal}, and the Q from germanium absorption, Q_{Ge}, as well as the total Q, $Q^{-1} = Q_{rad}^{-1} + Q_{metal}^{-1} + Q_{Ge}^{-1}$. The internal mode absorption efficiency is then given by Eq. (1).

$$\eta_{abs} = \frac{4Q^2}{Q_{Ge}Q_{rad}} \tag{1}$$

To extract each Q-factor, the signal ring-down is calculated and absorptive loss is successively added. First the radiation Q-factor is calculated with a simulation where all materials are made artificially lossless. The metal Q is calculated from the same simulation which has been run again but with a realistic absorptive aluminum metal. The total Q of that simulation is the reciprocal sum of the radiation Q and the metal Q. Finally the germanium Q is calculated by running a third identical simulation with both metal loss and absorptive loss from the germanium. The total Q in that simulation is the reciprocal sum of the radiation Q, metal loss Q, and germanium absorption Q.

To obtain the external coupling efficiency, an additional simulation is run where instead of sending the excitation through the waveguide, an point-dipole emitter is placed within the cavity to excite the cavity mode, and the optical power leaving through the waveguide, P_{wg}, is calculated and compared with the amount of optical power leaving to total simulation space, P_{tot} such that $\eta_{coup} = P_{wg} / P_{tot}$. In this calculation, all materials are made artificially lossless. Thus the quantum efficiency, disregarding current extraction, defect traps, and other electrical imperfections, is the product, $\eta = \eta_{abs}\eta_{coup}$.

3.1 MSM photodiode

Figure 3(a) shows the cross-sectional mode profile of the proposed MSM photodiode structure seen in Fig. 1. The electric energy density is presented in dB scale to show the strong enhancement of the field intensity inside the germanium region with respect to the incident light in the waveguide. In the case shown the quantum efficiency is calculated to be 36% for a resonant wavelength of 1530 nm. In addition it can be seen that very little of the electric field extends into the metal.

#194169 - $15.00 USD Received 22 Jul 2013; revised 3 Sep 2013; accepted 3 Sep 2013; published 16 Sep 2013

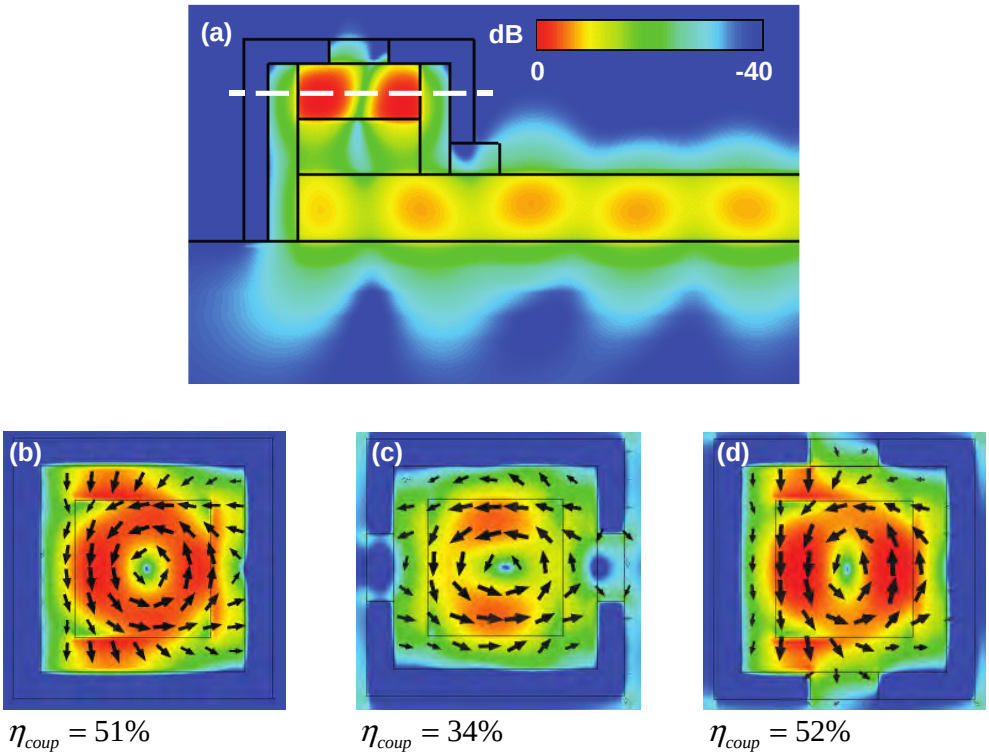

Fig. 3. (a) Shows the electric energy density of the resonant mode. (b) Electric field profile with completely enclosed metal box. (c) Electric field profile with the metal gap parallel to the waveguide, and (d) perpendicular to the waveguide.

The fundamental transverse-electric (TE) mode is operated in a given dimension, which originally has the doughnut electric-field profile, as shown in Fig. 3(b). Specifically the electric field is strongest in a doughnut ring around the interior of the germanium block. The electric field lines are parallel to the edge of the cavity. Because the germanium is electrically insulated from the silicon waveguide, all electrical contact must be made to the top or sides of the germanium. We examine the effect of separating the metal walls of the cavity to form top electrical contacts. In Fig. 3(b), the metal coating with no break is shown, and the mode is radially symmetric. In Fig. 3(c), the same mode is shown but with the break in the metal placed parallel to the waveguide, which causes the field to be enhanced parallel to the waveguide. This results in much poorer coupling between the waveguide and cavity mode, since the electric field lines of the cavity mode are mostly pointing perpendicular to the waveguide which leads to huge phase-mismatching. To fix this, the split in the metal is placed perpendicular to the waveguide, as shown in Fig. 1(a), and is the orientation used for the remainder of the paper. This orientation, shown in Fig. 3(d), enhances the electric field in the direction perpendicular to the waveguide, which is the same orientation as that of the waveguide mode, which greatly enhances the coupling efficiency of the cavity by creating a better mode overlap. Two key parameters are examined in investigating both how to optimize the device as well as fabrication tolerances. Specifically these are the nitride spacer thickness, which controls the coupling strength to allow for critical coupling, and the spacing between contacts, which is a more critical issue for fabrication.

The primary consideration is in Q-matching the structure such that the radiation and absorption rates of the cavity are made equal. This is the very same concept used to create critical coupling in ring resonators to waveguides [23]. It is assumed the majority of the radiation is due to the coupling with the waveguide structure. Since the coupling distance is

#194169 - $15.00 USD Received 22 Jul 2013; revised 3 Sep 2013; accepted 3 Sep 2013; published 16 Sep 2013

controlled directly by the thickness of the nitride spacer, altering this dimension in turn controls the radiation Q. Figure 4 shows the variation of the spacer layer thickness and its effect on radiation Q, absorption Q, and the overall quantum efficiency. It can be clearly seen that at the intersection of the radiation and absorption Q curves, the quantum efficiency reaches its peak of about 36%. In this case all other dimensions are as shown previously in Fig. 1(b). It should also be noted that as the spacer thickness becomes extremely thin, the cavity is over coupled to the waveguide, and the mode is not well defined, leading to less overall absorption and thus the higher absorption Q values. Once the cavity reaches critical coupling or under coupling, the absorption Q values remain relatively unchanged with respect to the spacer thickness. Overall this shows that the spacer thickness is fairly important to the proper coupling of the cavity mode, and that eliminating the spacer layer entirely would severely reduce the quantum efficiency.

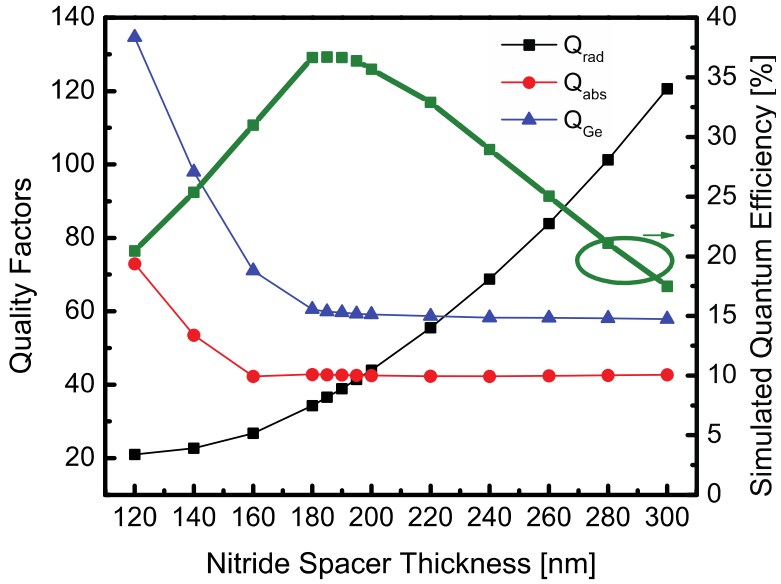

Fig. 4. Simulated quality factors and total quantum efficiency for a variation in the nitride spacer thickness demonstrates the critical coupling effect in this structure.

It should be noted that the spacer material does not need to be nitride. For example, silicon oxide can be used instead, allowing the use of much more common GOI substrate in fabrication. However because oxide has a lower index of refraction than nitride, the optimal oxide thickness will be less (150 nm). A secondary effect is that the cavity resonance blue-shifts, requiring a change in the germanium dimensions to maintain a resonance at the desired wavelength.

One other consideration is the separation between the contacts, which needs to be lithographically defined. Even with the best lithographic technology, sub-100nm lines are difficult to achieve without technologies such as e-beam lithography or focused ion beam lithography, both of which are undesirable for production lines. Shown in Fig. 5(a) is a variation of both the nitride spacer thickness and the contact separation. The total quantum efficiency is plotted, showing peaks due to critical coupling from the appropriate spacer thickness value. What can be seen is that while the quantum efficiency does increase slightly with a smaller gap and decrease slightly with a wider gap, overall the effect is that of a few percent in total efficiency, a total 4% change with a 150 nm variation in the gap dimension. More importantly the critical coupling condition does not change appreciably. This is encouraging for two reasons both related to fabrication. One is that it shows the gap can be

#194169 - $15.00 USD Received 22 Jul 2013; revised 3 Sep 2013; accepted 3 Sep 2013; published 16 Sep 2013

made rather wide to allow the use of standard DUV lithography. The other is that fabrication of such a device requires careful patterning of the sidewalls as well as that of the top. A slight variation in the gap, either on top, or on the sides should not greatly affect the optical performance.

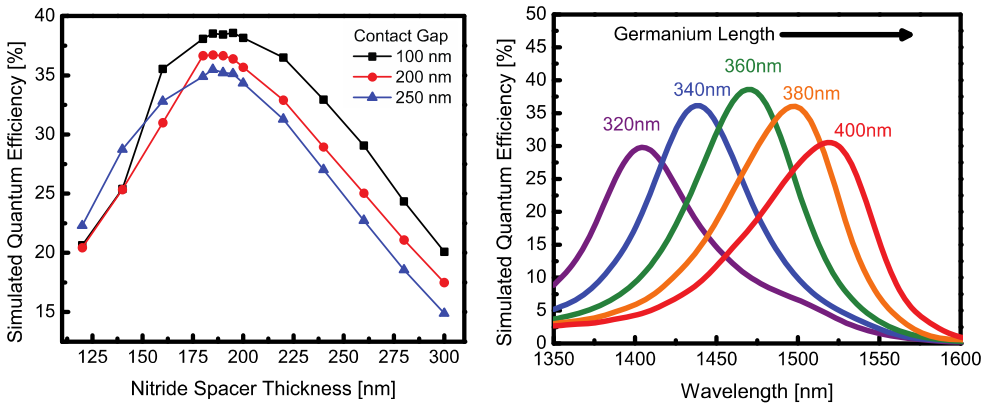

Fig. 5. (a) Simulated quantum efficiency plotted against spacer thickness and metal gap. (b) Resonant wavelength versus the lateral germanium dimensions, showing how the wavelength can be tailored.

Another large point of variation in the structure is that of the germanium dimensions. Figure 5(b) shows the variation of length of the germanium block, while all other dimensions are kept constant. What is shown is that as expected the resonance red-shifts when the dimensions are lengthened, and blue-shifts when shrunk. The effect is rather linear, and a line of best fit can be applied to give an expression relating the resonant wavelength with the dimension. The fit shows that the cavity dimensions are roughly a half-wavelength of the resonant wavelength. This emphasizes that the resonance is the fundamental mode of a dielectric cavity and that the metal is simply acting as a reflector rather than creating a plasmonic mode.

3.2 Vertical p-i-n photodiode

The p-i-n design has the same doughnut mode, whose electric field profile is identical to that of Fig. 3(a). However there are a few key differences which are displayed in Fig. 6. Primarily the coupling efficiency is much higher (>60%) compared to the MSM cavity for two reasons. In the MSM cavity, the light is radiated both through the gap between the metals, and through the base into the substrate. Thus much of light escapes before it can be captured by the cavity mode. With the p-i-n design, there is no gap in the metal, eliminating one form of coupling loss. Because the p-i-n design has silicon waveguides on the side of the cavity for electrical contacts, a portion of the light that would enter the substrate actually couples into these waveguides, as in Fig. 6(b). If these contact waveguides are properly designed, this light when reflected back from them will couple very well to the cavity mode and is in a sense recycled. Further coupling improvements would likely require asymmetry in the oxide cladding on the sides of the cavity [11], something which is not realistic with present fabrication technology. Another important aspect seen in the p-i-n cavity is that the majority of the mode is present in the upper portion of the germanium. This is very important from a practical standpoint since with the current germanium growth technology, the first 50-100 nm of germanium grown on silicon is typically quite poor and thus would have many defect states present [5]. This defective layer of germanium could be doped so that it is not a part of the intrinsic absorbing layer.

#194169 - $15.00 USD Received 22 Jul 2013; revised 3 Sep 2013; accepted 3 Sep 2013; published 16 Sep 2013

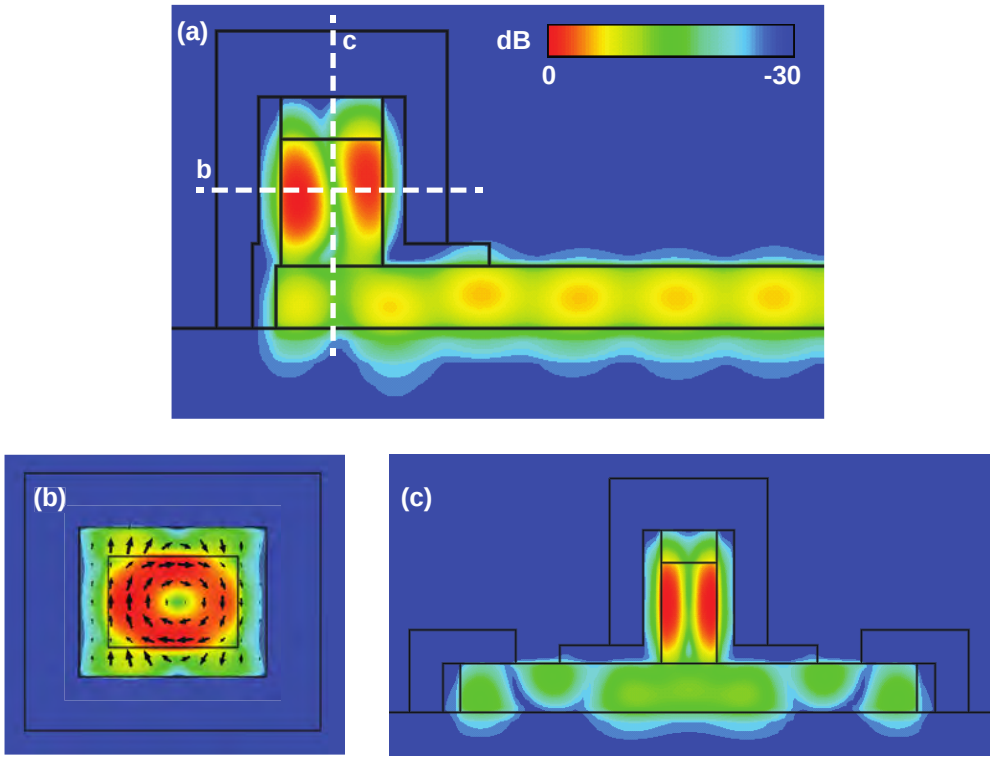

Fig. 6. (a) Side-profile of the electric energy density in dB scale. (b) Electric energy density slice with electric field vectors showing similar doughnut mode. (c) Electric energy density of slice of the device showing the side silicon waveguide contacts.

To match the absorption Q for critical coupling there needs to be a way to adjust the radiation Q of the cavity. In the MSM design this was achieved with the nitride spacer thickness, however in the p-i-n design, there is no spacer between the germanium and silicon waveguide. In this case both the poly-silicon top contact and the total germanium thickness control the radiation Q such that increasing the germanium thickness will increase the radiation Q, shown in Fig. 7. What makes this more complicated than in the MSM design is that the total germanium dimensions are strongly tied to the resonance wavelength. Making the germanium thicker will red-shift the wavelength. Thus care must be taken to properly choose the length and width dimensions so that the proper radiation Q can be obtained at the desired wavelength. The fact that the length and width dimensions can alter the wavelength is shown in Fig. 8(b).

#194169 - $15.00 USD Received 22 Jul 2013; revised 3 Sep 2013; accepted 3 Sep 2013; published 16 Sep 2013

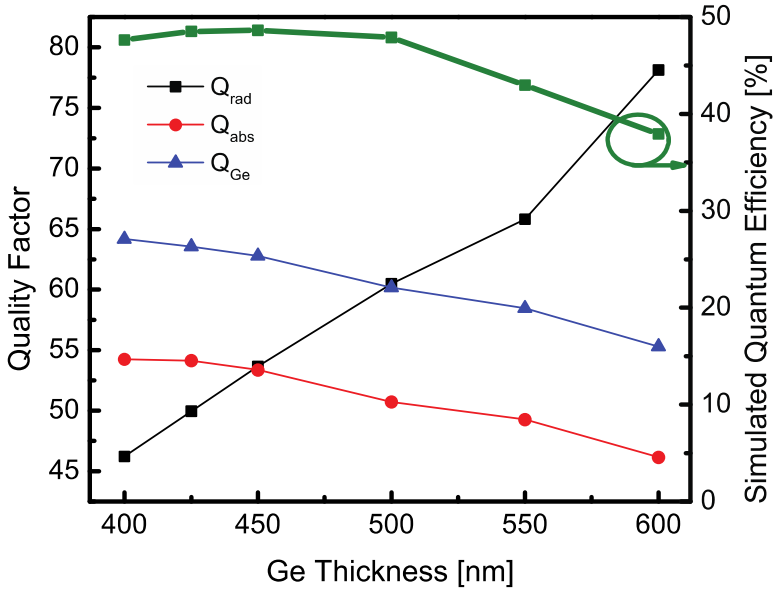

Fig. 7. Matching the absorption and radiation Q by altering the germanium thickness.

Additionally as in the MSM device, the cladding thickness strongly affects the coupling and the amount of mode overlap with the metal. A thinner cladding will provide better coupling efficiency but at the cost of higher electric field penetration into the metal and thus higher metal loss. Thus a middle ground must be achieved between the two. For this cavity at 1500 nm wavelength that is about 80 nm.

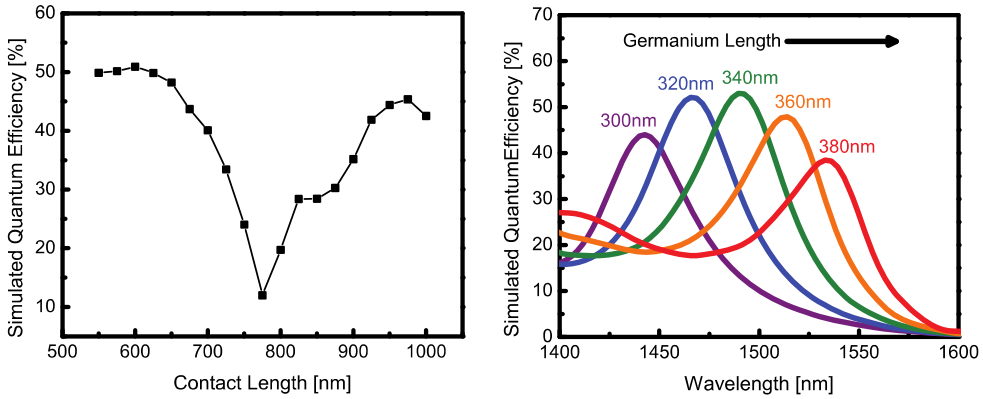

Fig. 8. (a) Simulated quantum efficiency as a function of the silicon contact length dimensions as well as (b) how to tune the resonant wavelength by changing the germanium lateral dimensions.

As was previously mentioned, the length of the contact waveguides strongly affects the coupling efficiency in with the cavity. Specifically, the cavity also couples to these waveguides, and thus light from the input waveguide that does not immediately couple to the cavity mode with spread into these side waveguides. If their length is properly chosen, when this light reflects back from the end of them and reaches the cavity again, it will couple into the cavity. However if when the light makes its return trip from the end of the side waveguide it does not overlap with the mode then destructive interference will occur dramatically reducing the coupling efficiency. This is shown in Fig. 8(a). Taking this into account, it can

#194169 - $15.00 USD Received 22 Jul 2013; revised 3 Sep 2013; accepted 3 Sep 2013; published 16 Sep 2013

be seen that by matching the Q factors, and choosing the proper contact length the p-i-n device can easily achieve over 50% quantum efficiency from simulations.

For a true p-i-n device, the polysilicon top contact, and underlying waveguide must both be heavily doped to allow good contact resistance. In the simulations it is assumed both silicon structures are doped to $5x10^{19}$ cm^{-3}, which gives a free carrier absorption of about 300 cm^{-1} at 1500 nm wavelength [21]. The excess loss caused by this doping was lumped into the Q_{metal} loss term, and indeed factors into the Q matching of the structure. However as can be seen from the electric energy density in Fig. 6, compared to the germanium itself, very little energy is present in either part of the silicon. Combined with the fact that the germanium has an absorption coefficient of 2000 cm^{-1} at 1500 nm, there is very little net effect from the silicon doping at these levels. Comparative simulations show a 2-3% increase in total absorption efficiency when the free carrier absorption is removed from the silicon in the structure. Additionally the reality of the film quality of the aluminum can affect absorption performance. In general, evaporation and sputtering can produce very smooth films, but aluminum is known to form a 2-5 nm interfacial oxide under even high vacuum conditions [20]. The effect of this thin Al_2O_3 layer between the aluminum and SiO_2 cladding the germanium is minimal. Aluminum oxide has a negligible absorption coefficient at 1500 nm, and the index of refraction (n = 1.75) is comparable to SiO_2 (n = 1.45). To design for such a layer, one would deposit 3-7 nm less SiO_2 around the device. However such considerations would need to be calibrated against specific aluminum deposition systems.

4. Discussion

It may appear that the p-i-n device presented is a great improvement over the MSM device from a quantum efficiency and capacitance standpoint. There are several other factors to consider that may make the MSM device more attractive. From an energy efficiency perspective, the higher quantum efficiency and lower capacitance of the p-i-n device are highly desirable as they reduce the ultimate number of photons per bit for communication in a receiver circuit. However also consider the total thickness of the germanium layer. For on-chip photoreceivers, generally we do not want the bias voltage on the photodiode to be very large, while having a large field across the photodiode can greatly enhance responsivity through faster carrier collection and extending the bandgap through the Franz-Keldysh effect [24]. By using the electric breakdown of germanium, which occurs at 100 kV/cm, we can estimate the maximum useful voltage one might apply to these devices, which is summarized in Table 1. Specifically with a gap between metal contacts of 200 nm in the MSM device, the maximum voltage that could be applied before breakdown is 2V. This also implies that this device could utilize these high field effects from a relatively low operating voltage, and one that is significantly lower than that of the p-i-n device. Similarly, due to its smaller dimensions between electrical contacts, the MSM device should be significantly faster than the p-i-n device. A back of envelope calculation on transit time can be done for each device assuming in the MSM case the carriers must at a maximum travel from under one contact to the other contact (250 nm) and in the p-i-n device the carriers at maximum must travel completely across the intrinsic region (450 nm). Using the saturated electron drift velocity since holes move faster in germanium, we arrive at a minimum transit time of 5 ps for the MSM device and 9 ps for the p-i-n device. Since both devices have such small capacitances, both are very likely to be transit time limited in their operation speed, and so a factor of two difference in transit time would mean that the MSM device could likely be twice as fast as the p-i-n device. A more practical consideration in comparing the two devices comes in terms of fabrication. The MSM device with the germanium on oxide could be obtained either through current GOI techniques or with the more recent rapid melt growth technique, which is relatively cheap and fast, requiring CVD or sputtering deposition of germanium followed by a quick RTA step. The p-i-n device by having the germanium directly on silicon requires

#194169 - $15.00 USD Received 22 Jul 2013; revised 3 Sep 2013; accepted 3 Sep 2013; published 16 Sep 2013

epitaxy, which can be expensive and slow. However at this level of conjecture the tradeoffs between the two growth methods are extremely difficult to quantify.

Table 1. Summary of key parameters simulated and calculated from the two designs presented.

	MSM Device	*p-i-n Device*
Quantum Efficiency	39%	51%
Capacitance	<200 aF	<100 aF
Germanium Thickness	180 nm	450 nm
Minimum Carrier Transit Time	5 ps	9 ps
Maximum Voltage	2 V	4.5 V
Germanium Growth	GOI or Rapid Melt Growth	Direct Epitaxy on Silicon

Finally if one is interested in purely increasing the quantum efficiency of either device, metal loss will become an issue, especially since aluminum is rather strongly absorbing near 1500 nm. A less lossy material such as gold or silver can be used instead, which should increase the total efficiency slightly (>61%), but at the sacrifice of using solely CMOS compatible materials. Additionally, one could choose to use III-V material instead of germanium as the absorber which would also increase the quantum efficiency but at the cost of possible CMOS compatibility. However if III-V lasers were to be integrated into CMOS as was recently proposed [25], then it is not unreasonable to use the same highly absorbing material for the photodetector as well.

5. Conclusions

We have proposed both MSM and p-i-n device designs for sub-fF germanium photodiodes. Backed by theory and simulations, the MSM photodiode has 39% quantum efficiency with <200 aF capacitance, while the p-i-n photodiode has 51% quantum efficiency with <100 aF capacitance. Both devices utilize a single-mode cavity resonance and couple directly to a silicon waveguide, while using only CMOS compatible materials for the possibility of monolithic silicon photonics integration. When coupled with an appropriately designed receiver circuitry, these low-capacitance photodiodes should yield extremely sensitive photodetectors allowing for ultra-low energy photonic links.

Acknowledgments

We would like to acknowledge funding through the National Science Foundation Center for Energy Efficient Electronics Science (E3S) under NSF Award 0939514. National Science Foundation Center for Integrated Access Network (CIAN) under grant #EEC-0812072, Intel, the NSF Graduate Fellowship (DGE 1106400) and NDSEG Graduate Fellowship. The authors would also like to thank Amit Lakhani, Tae Joon Seok, and Michael Eggleston for very valuable discussions.

#194169 - $15.00 USD Received 22 Jul 2013; revised 3 Sep 2013; accepted 3 Sep 2013; published 16 Sep 2013